

RSC Advances



This is an *Accepted Manuscript*, which has been through the Royal Society of Chemistry peer review process and has been accepted for publication.

Accepted Manuscripts are published online shortly after acceptance, before technical editing, formatting and proof reading. Using this free service, authors can make their results available to the community, in citable form, before we publish the edited article. This *Accepted Manuscript* will be replaced by the edited, formatted and paginated article as soon as this is available.

You can find more information about *Accepted Manuscripts* in the [Information for Authors](#).

Please note that technical editing may introduce minor changes to the text and/or graphics, which may alter content. The journal's standard [Terms & Conditions](#) and the [Ethical guidelines](#) still apply. In no event shall the Royal Society of Chemistry be held responsible for any errors or omissions in this *Accepted Manuscript* or any consequences arising from the use of any information it contains.

Cite this: DOI: 10.1039/c0xx00000x

www.rsc.org/xxxxxx

ARTICLE TYPE

Field emission properties of highly ordered low-aspect ratio carbon nanocup arrays

Bipin Kumar Gupta^{a,*}, Garima Kedawat^b, Pawan Kumar^{a,c}, Satbir Singh^{a,c}, Sachin R. Suryawanshi^d, Neetu Agrawal (Garg)^b, Govind Gupta^a, Ah Ra Kim^e, R. K. Gupta^f, Mahendra A. More^d, Dattatray J. Late^{g,*}, Myung Gwan Hahn^{e,*}

Received (in XXX, XXX) XthXXXXXXXXXX 20XX, Accepted Xth XXXXXXXXXXXX 20XX

DOI: 10.1039/b000000x

Herein, we design and develop a field emission device utilizing highly porous carbon nanocup (CNC) films. These three-dimensional (3D) low-aspect ratio CNC structures were fabricated by a combination of anodization and chemical vapor deposition techniques. The low turn-on fields of 2.30 V/ μm were observed to draw an emission current density of 1 $\mu\text{A}/\text{cm}^2$ and a maximum emission current density of $\sim 1.802 \text{ mA}/\text{cm}^2$ is drawn at an applied field of $\sim 4.20 \text{ V}/\mu\text{m}$. The enhanced field emission behavior observed from the CNC films is attributed to excellent field enhancement factor of 1645. The observed field emission properties of CNC arrays are attributed synergistic combination of high aspect ratio, nano-sized radius of curvature, highly organized distribution of the emitters over the whole area of specimen and lower screening effect of the CNC arrays. These observations shed light on the effect of the stacking carbon layers of CNC on their electronic properties and open up possibilities to integrate new morphologies of graphitic carbon in nanotechnology applications. Thus, the low turn on field, high emission current density and better emission current stability enables CNC based future field emission applications.

1. Introduction

Field-electron emission is a form of quantum mechanical tunneling in which electrons pass through a barrier in the presence of an electric field¹. This phenomenon is highly dependent on both the physical characteristics of the material and the shape/structure of the particular cathode, so that high-aspect ratios (height/tip radius) structures produce higher field-emission currents at lower applied electric fields^{2,3}. It is necessary to grow vertically aligned nanostructure arrays on a large scale with suitable emitter current density with high-aspect ratio. However, current technologies are significantly limited by the difficulty of tailoring morphology and aspect ratio of individual nano-scaled units. Carbon-related nanomaterials such as carbon nanotubes (CNTs)^{4,5}, carbon nanocups^{6,7} and graphene^{8,9} have gained importance for promising candidates as field electron emitters to be used in futuristic cold-cathode flat panel displays and various vacuum microelectronic devices. Recently, carbon nanocup (CNC) composed of carbon stacked layers have attracted increasing attention due to the low aspect ratios, good thermal and electrical conductivity, and robust chemical and mechanical stability, serve as a special and functional nanosized material in heterogeneous catalysis, solar cells, etc^{10,11}. The field enhancements observed in reduced graphene oxide -TiO₂ hybrid structure nano-arrays in our recently published paper attributing to the contribution of low work function with nonrectifying barriers³. Field emission would need high density and well-

ordered carbon nanotubes arrays. Although, several oxide based nanostructures are well studied and reported in literature in last few years.¹²⁻¹⁴

Especially, CNC arrays exhibit several favorable characteristics as an electron source, such as small radius of curvature, outstanding chemical inertness, exceptional thermal stability, and high mechanical strength. CNC films incorporated with millions of truncated conical graphitic structures, different from conventional CNTs made up of multi-seamless cylinders of hexagonal carbon networks.^{6,15} The cup-like nano-structure provides a hollow tubular morphology. It differs from other quasi- one dimensional (1D) carbon structures, which normally behave as quasi-metallic conductors of electrons. Some of 1D carbon structures exhibit semiconducting behaviors due to their chirality.¹⁶ Such structure provides a large portion of exposed and reactive edges with abundant dangling bonds both on the outer surface and in the inner channel. Additionally, the chemical activity of the inner channel is even higher due to highly strained curvature.¹⁷ Therefore, the utilization of these exposed edges of CNCs to chemical functionalization or surface modification opens up new avenues in absorbent materials, composites, field emitters and gas storage components. For the practical application to field emission sources, the growth of periodic array of CNCs on a large area with high packing density is necessary. CNC has low-aspect ratio (1:1.2) showing good emission performance with flat thin film nature which is highly required in FED based display panels; it has been shown in our experiment,

RSC Advances Accepted Manuscript

which has not been reported earlier. In recent years, anodic aluminum oxide (AAO) nano-templates based approaches have been widely introduced to fabricate well-aligned periodic arrays of nanostructure.

Herein, we proposed and demonstrated a high performance field emission device with vertically aligned 3D and low aspect-ratio CNCs structure. The highly organized CNC arrays were grown by chemical vapor deposition (CVD) using a short channel AAO template. Figure 1 shows a schematic diagram of the fabrication approach for CNC films with their counterparts of scanning electron microscope (SEM) image and appearances of the as-grown sample. The simple field emission device utilizing CNC films was fabricated as shown in schematic drawing (Figure 1). The field emission measurements showed that carbon nanocup arrays-based field emission device had outstanding performance although these have low-aspect ratio. It is suggested that the open edges on the CNCs act as active emission sites in vertically aligned 3D CNC structure giving enhanced emission characteristics.

2. Experimental

2.1 Synthesis of low-aspect ratio carbon nanocup films

The direct deposition of dispersed CNTs onto a 3D substrate is simple and effective to construct porous architectures. AAO template with continuous 3D surface and good mechanical flexibility can serve as a supporting substrate. Nano-sized porous aluminum oxide templates (AAO) were fabricated using a standard electrochemical anodization technique. To create highly organized arrays of nanopores, two-step anodization process was conducted. In the first anodization process, a high purity aluminum (Al) foil was anodized at 35 V for 6 hours in 3% oxalic acid ($C_2H_4O_2$) solution at room temperature. The anodized Al foil was placed in the solution containing a mixture of 3% phosphoric (H_3PO_4) and 3% chromic (H_2CrO_4) acids for 18 hours to remove the formed aluminum oxide layer. Then, a second anodization process was conducted for 30 seconds to fabricate highly ordered short nanochannels. The samples were soaked in a 3% phosphoric acid solution for 1 hour for widening of nanopores. With this sample, we performed chemical vapor deposition (CVD) process to synthesize low aspect ratio carbon nanocup structure inside AAO template. The fabricated AAO templates were placed in a quartz tube and evacuated using rotary pump. Then, high purity argon gas was introduced as a carrier gas during heating. When the temperature reached at 660 °C, acetylene (25 sccm)-argon (200 sccm) mixture gas was supplied as a carbon source for 45 min for the deposition of a graphitic carbon layer inside predesigned short AAO nanochannels resulting in the connected arrays of carbon nanocup film structure. Carbon nanostructures inside of AAO were released by dissolving the AAO template in 33% hydrofluoric acid solution for as deposited nanocup. Our approach for fabricating these carbon nanocup structures is shown schematically in Figure 1 with the schematic of the field emission measurement for CNC film. This Figure illustrates the fabrication process with their counterparts of SEM images and

appearances of the as-grown sample. First, the CVD process synthesized the highly porous carbon nanocup structure on AAO template, then AAO template was dissolved using hydrofluoric acid solution and resulting the three-dimensional porous architectures of a connected arrays of carbon nanocup film was formed.

Under the above-explained experimental conditions of synthesis using CVD method, the formation of carbon nanocup can be explained by the controlled growth of graphene films in the predesigned AAO nanochannel template. At the temperature of around 660°C, carbon atoms begin to be adsorbed on the substrate and the graphene islands begin to nucleate. This leads to the formation of flat epitaxial graphene sheet on the AAO template. Since the graphene growth consumes carbon atoms, thus the carbon source supply is done for a judiciously calculated period of time. As soon as, the carbon concentration is below super saturation, the nucleation and growth of graphene islands would be finished.

2.2 Characterization

X-ray diffraction (XRD) studies of the powder samples have been carried out using Rigaku, Miniflex, $CuK\alpha_1$; $\lambda = 1.5405 \text{ \AA}$. Prior to the XRD measurement, the diffractometer was calibrated using silicon powder as the reference material ($d_{111} = 3.1353 \text{ \AA}$). Raman studies were carried out using an argon ion laser with a wavelength of 514 nm as the excitation source (Model Innova 70, Coherent). The XPS analysis was carried out in an ultra-high vacuum (UHV) chamber equipped with a hemispherical electron energy analyzer (Perkin Elmer, PHI1257) using non-monochromatized Al $K\alpha$ source (excitation energy of 1486.7 eV) with a base pressure of 4×10^{-10} torr at room temperature. The surface topography was characterized from the scanning electron microscopy (SEM) image using a microscope of Carl ZEISS-SUPRA 40 at 5 kV operating voltage. The microstructural studies were carried out using high-resolution transmission electron microscopy (HRTEM, Model No. Technai G20-twin, 300 kV with super twin lenses having a point and line resolution of 0.144 nm and 0.232 nm, respectively).

2.3 Field emission measurements

The field emission current density (J) versus applied electric field (E) and emission current (I) versus time (t) characteristics were measured in a planar 'diode' configuration at base pressure of $\sim 1 \times 10^{-8}$ mbar. A typical 'diode' configuration consist of a phosphor coated semitransparent screen (a circular disc having diameter ~ 40 mm) as an anode. In order to investigate the FE, very small quantity of CNCs film were pased on stainless steel holder by using silver paste (radius $\sim 1 \text{ cm}^2$), which was then mounted in the parallel plate diode assembly. The was held parallel with an anode screen in close proximity. The ultra high vacuum chamber is equipped with rotary backed turbo molecular pump, sputter ion pump and titanium sublimation pump. For achieving base pressure of $\sim 1 \times 10^{-8}$ mbar, the chamber is baked at 200°C for 12 hrs. The FE measurements were carried out at fixed

cathode-anode separation of ~ 1 mm. The emission current was measured on Keithley Electrometer (6514) by sweeping dc voltage applied to cathode with a step of 40 V (0-40 kV, Spellman, U.S.). The field emission current stability is

investigated using computer controlled data acquisition system with sampling interval of 10s. Field emission micrographs before field emission measurements cathode surface cleaning processes,

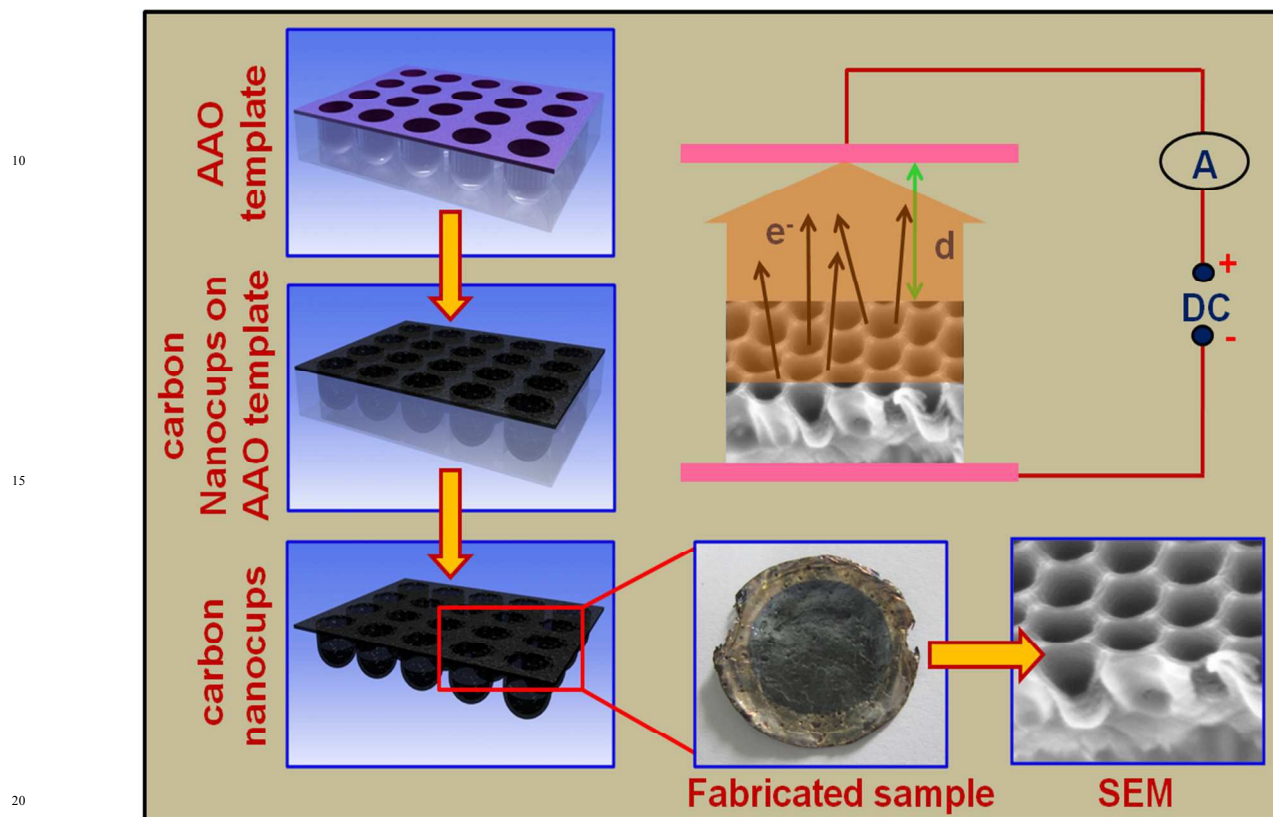


Fig. 1: Schematic illustrating the fabrication process with their counterparts of SEM images and appearances of the as-grown sample; the scale bar is 100 nm. First, the chemical vapor deposition (CVD) process synthesized the highly porous carbon nanocup structure on AAO template, then AAO template was dissolved using hydrofluoric acid solution and resulting the highly ordered three-dimensional porous architectures of a connected arrays of carbon nanocup film was formed with thickness ~ 1 mm. And schematic of the field emission measurement set-up for carbon nanocup (CNC) film; the scale bar is 100 nm.

such as thermal cleaning or field evaporation were not employed. Special care was taken to avoid any leakage current using shielded cables and ensuring proper grounding. Before recording the FE measurements, pre-conditioning of the cathode was carried out by keeping it at ~ 1000 volts so as to remove loosely bound particles and/or contaminants by residual gas ion bombardment.

3. Results and discussion

The structural characterizations of as-synthesized highly ordered CNC arrays were conducted by using X-ray diffraction (XRD) and Raman spectroscopy. The XRD pattern of the CNCs is shown in Figure 2a, which indicates the existence of aluminium (Al) recorded from AAO template and graphitic carbon lattice. It exhibits one broad peak and two more sharp peaks centered at

25.7° , 45.2° and 50° signifying the formation of hexagonal carbon lattice (JCPDS no. 75-1621) with estimated lattice constants $a = 2.467 \pm 0.008 \text{ \AA}$ and $b = c = 6.793 \pm 0.011 \text{ \AA}$ as compares to the standard lattice parameters $a = 2.470 \text{ \AA}$ and $b = c = 6.790 \text{ \AA}$. A broad small diffraction peak appeared at 25.7° (as shown by blue colored dashed square) corresponding to the graphite plane (002) with an interlayer spacing (0.34 nm) of the nanotubes.¹⁸ The magnified view of this peak is also shown in Figure 2b. However, low intense peak at 45.2° has been identified as an Al cubic structure (JCPDS no. 03-0932), which indicates the nanocup synthesized on the AAO template in the synthesis process. To elucidate the graphitic structure of CNCs, Raman spectroscopy was conducted with a 514 nm wavelength laser in a spectral range of $600\text{--}2200 \text{ cm}^{-1}$. The Raman spectrum recorded from CNC film clearly exhibits two well-defined sharp peaks, indicating sp^2 and sp^3 bonds of the graphitic structure.

Cite this: DOI: 10.1039/c0xx00000x

www.rsc.org/xxxxxx

ARTICLE TYPE

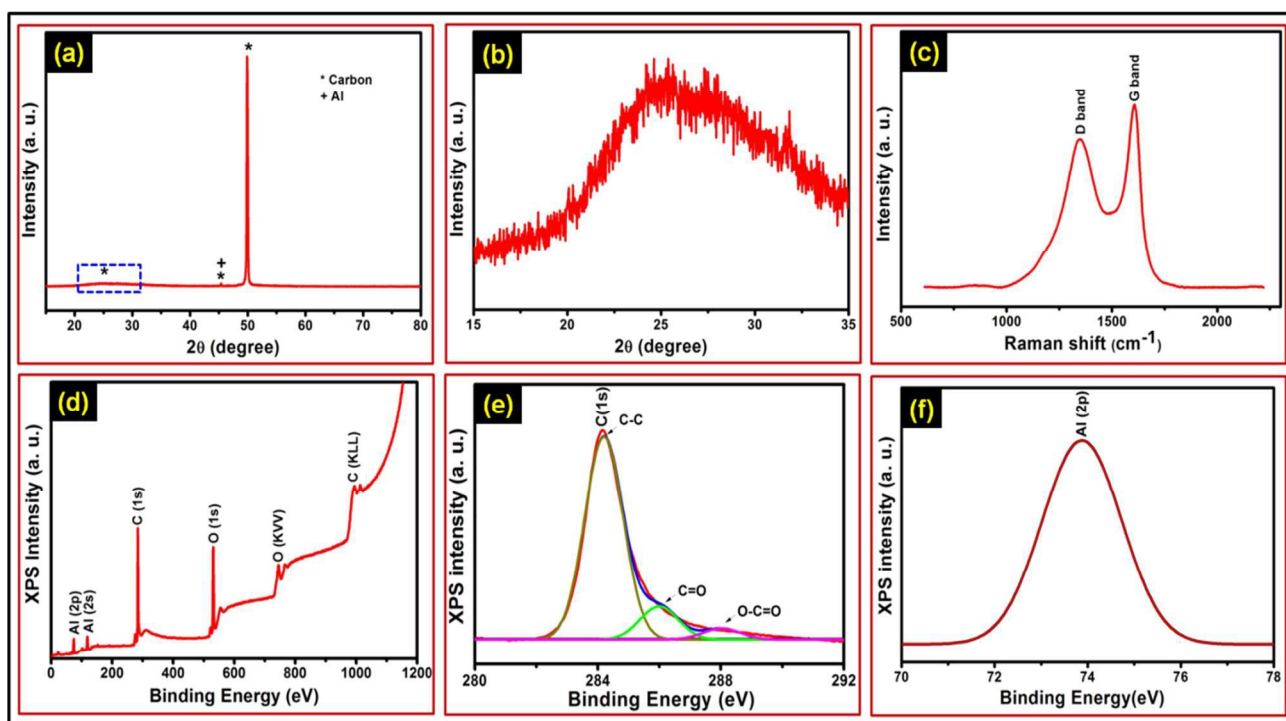


Fig. 2: (a) XRD pattern of carbon nanocup; * represents the carbon lattice plane and + signifies the aluminium lattice plane, (b) enlarge view of fig. a, which has been marked by blue colored dashed square in fig. a, (c) Raman spectrum (using 514 nm wavelength laser probe) of carbon nanocup; their A_D/A_G ratio is 0.81, (d) XPS survey scan spectrum of carbon nanocup, (e) high resolution spectra of C 1s region of XPS spectrum of carbon nanocup and (f) high resolution spectra of Al 2p region of XPS spectrum of carbon nanocup.

The D band at 1350 cm^{-1} (the disorder-induced band), and G band at 1600 cm^{-1} (the tangential modes of graphitic structures) are typically presented in graphitic structures and their A_D/A_G ratio is 0.81, indicating the high degree of disorder on the as-synthesized CNC structure due to catalyst-free CVD process. Also, the G band represents the in-plane stretching vibrations of the sp^2 -carbon-carbon bonds within the ordered graphitic layers of CNCs.^{16,19,20} The synthesized cup-like carbon nano-structures are comprised of multi-layered graphitic layers. X-ray photoelectron spectroscopy (XPS) clearly revealed the presence of carbon, oxygen, and aluminum elements of CNC films as shown in Figure 2d. To determine the chemical component and the oxidation state of carbon element, high-resolution XPS spectra of C1s are curve-fitted into three contribution peaks appearing at 284.2, 286.0 and 288.0 eV (Figure 2e). The main peak at 284.2 eV is assigned to sp^2 -hybridized graphite-like carbon atoms (C-C bond). The peaks at 286.0 and 288.0 eV are typical of carbon atom bound to one oxygen atom by double bond (C=O bond) and to two oxygen atoms (O-C=O bond), respectively.²¹ It signifies that the oxygen-containing functional groups are sequentially introduced onto the surfaces of the tubes. The core level peak of

the Al (2p) region for CNCs is also shown at 78.6 eV binding energy in Figure 2f. The presence of Al element is due to the AAO templates.

The scanning electron microscope (SEM) and transmission electron microscope (TEM) micrographs of a highly organized CNC structures after removing the AAO template are shown in Figure 3. The SEM images of top view of CNC arrays (Figure 3a) and side view of CNC arrays (Figure 3b) clearly show their low-aspect ratio structures with a cup diameter of $\sim 100 \pm 2\text{ nm}$ and length of $\sim 120 \pm 2\text{ nm}$. The CNC arrays have a well-organized, interconnected structure and a highly porous surface morphology with very sharp edges (thickness $\sim 5\text{--}10\text{ nm}$) on a diameter. This highly porous, low-aspect ratio nanocup structure provides a large specific surface area, which indicates that the walls of vertically aligned CNTs give exuberance of surface in nanocup.^{6,20} The additional surface area on the CNC nano-structure enhances the electrochemical properties and optical properties of devices by providing a large area for the electrolyte ions to interact with the electrode surface.

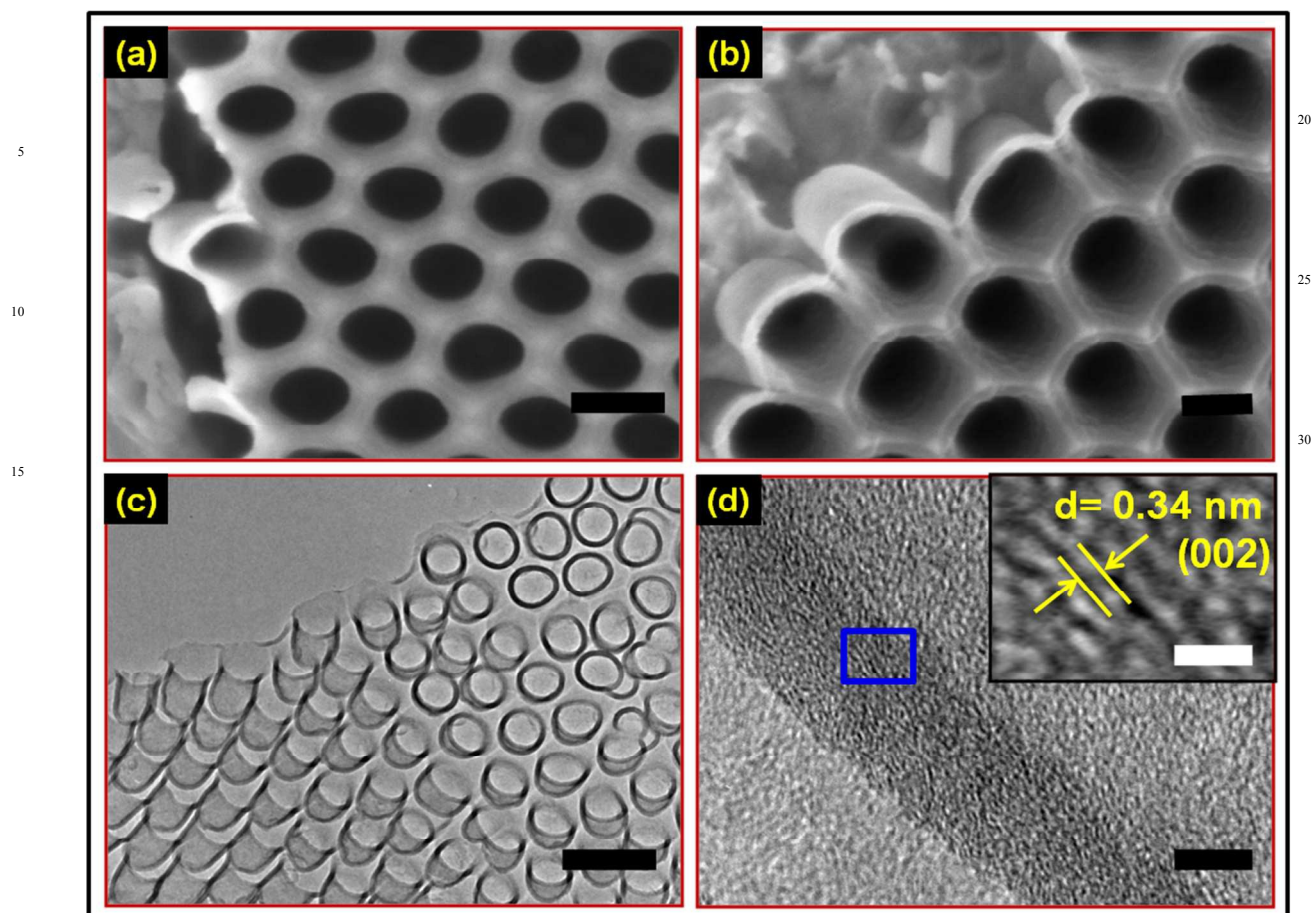


Fig. 3: SEM and TEM micrographs of a CNC film structure. SEM images show (a) top-view of CNC array on the AAO template; the scale bar is 100 nm, (b) side-view of CNC film on the AAO template, the scale bar is 100 nm; these images show clearly their low-aspect ratio hollow structures having $\sim 100 \pm 2$ nm diameter and $\sim 120 \pm 2$ nm length, TEM image shows (c) connected arrays of CNC film after removing of the AAO template, the scale bar is 100 nm and (d) HRTEM image of CNC, the image shows the graphitic structure of CNC is defective and inset shows its magnified view; which has been taken from the blue square region.

The top view morphology for another CNCs sample has also investigated (Figure S1; see Supporting Information). The TEM image of connected array of CNCs (Figure 3c) has a large hollow core along their length with ~ 100 nm inner diameter and ~ 120 nm length demonstrates the formation of wide scale CNCs. The high-resolution TEM (HRTEM) image is shown in Figure 3d and inset shows its magnified view; which has been taken from the blue square region. It reveals the graphitic layers of CNCs corresponding to (002) plane with an interplanar spacing of 0.34 nm. Since CNCs exhibit enormously active diameter with sharp edges.

The template-assisted synthesis of the CNCs can be controllably grown by the chemical vapour deposition. The CNC films have numerous sharp edges and enormous proportion of nano-protrusions. Due to the unique morphology of the nanocups, field emission performance should be enhanced. The field emission measurement instrument is shown in Figure S2 (see supporting information). In the electron field emission experiments, the cathode was the supported CNTs film and the

anode was a probe (0.63 mm in diameter) positioned at a distance $d \sim 1$ mm above the surface. The cathode connection was via the CNC film. The samples were mounted on a ceramic holder in a high vacuum chamber. After the chamber reached a base pressure below 5×10^{-5} Pa and the field emission was initiated by cycling the voltage applied to the probe up to 1000 V for five times. After a pause of about 0.5 h at zero electric field, the field emission current was recorded as a function of voltage (V) applied to the probe. The Fowler-Nordehim ($F-N$) equation for field emitters deposited on flat substrates in the form of thin film, has been modified to yield an equation in terms of current density (J) and the applied electric field ($E = V/d$, where V is the voltage applied between the flat cathode and the anode screen, and d is their separation). The modified $F-N$ equation is as follows,²²⁻²⁵

$$J = \lambda_M a (\beta^2 E^2 / \Phi) \exp(-b \Phi^{3/2} v_F / \beta E) \quad (1)$$

where, λ_M is macroscopic pre-exponential correction factor, $a = (1.54 \times 10^{-6} \text{ AeV V}^{-2})$ and $b = (6.83 \text{ VeV}^{-3/2} \text{ nm}^{-1})$ are constants, Φ is the work function, β is field enhancement factor and v_F (correction factor) is a particular value of the principal Schottky-Nordheim barrier function. The plot of the field emission current

density (J) versus applied electric field (E) for CNC films is shown in Figure 4a. As the field emission behaviour is directly dependent on the relative dimensions of the emitter, CNCs with very small thickness ~ 5 -10 nm (sharp edges) and having the depth of ~ 100 -150 nm are expected to be good field emitters. The turn-on and threshold field, defined as the field required drawing an emission current density of $\sim 1 \mu\text{A}/\text{cm}^2$ and $\sim 10 \mu\text{A}/\text{cm}^2$, is found to be $2.30 \text{ V}/\mu\text{m}$ and $\sim 2.50 \text{ V}/\mu\text{m}$, respectively for CNC arrays. As the applied voltage is increased further, the emission current is found to increase very rapidly and an emission current density of $\sim 1802 \mu\text{A}/\text{cm}^2$ is drawn at an applied field of $\sim 4.20 \text{ V}/\mu\text{m}$, indicating field emission is as per as F-N theory.

Furthermore, the field emission behaviour of CNC sample 55 from 1st to 6th cycle runs are shown in the Figure S3a (see supporting information). All tested samples show better emission uniformity and a good reproducibility of field emission behaviour during the initial 6 cycle run. In addition to the cyclability test, the field emission characteristics of different as-synthesized CNC samples (sample 1, sample 2, sample 3, sample 4 and sample 5) are also examined to explore reproducibility and the results are shown in Figure S3b (see supporting information). It can be noticed that all the samples are showing almost similar and consistent behaviour.

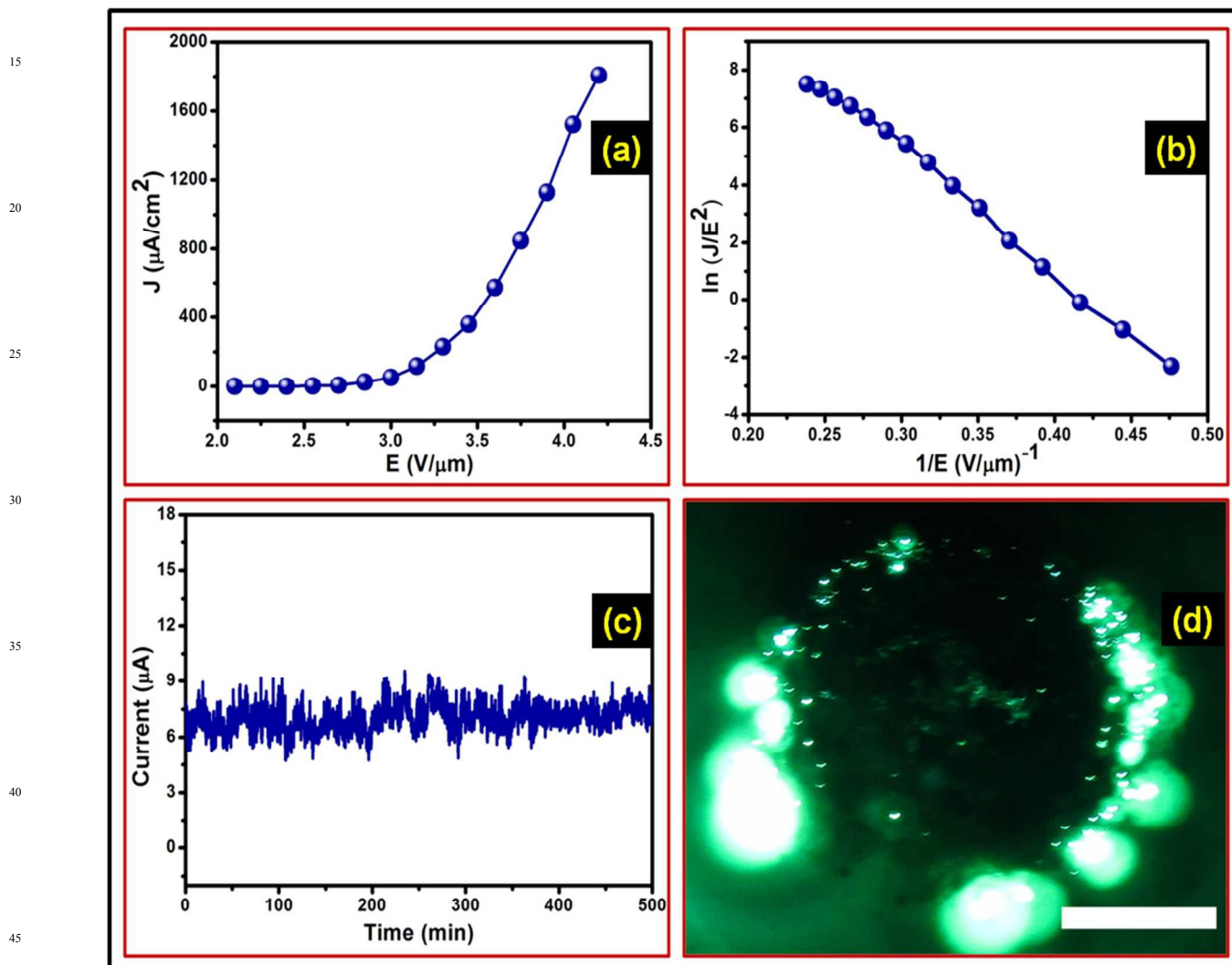


Fig. 4: (a) applied electrical field as a function of emission current density, (b) F-N plot showing nonlinear behavior indicating field emission from the CNC film emitter, (c) long term field emission current stability indicating fairly stable emission current and (d) field emission pattern taken during the long term stability study of the emitter, the scale bar is 1 cm.

In the case of CNC films, emission occurs from multiple emitters and an integrated current is measured. There could be lots of variations in local fields due to various geometries of the emitters. Also, the exact analysis of field emission characteristics of CNC arrays is difficult owing to work function of each emitter is not necessarily same. However, it may be noted that CNCs provide a hollow tubular morphology unlike that of conventional CNTs, which are made up of seamless cylinders of hexagonal carbon network. Compared to nanotubes, the nanocups have a greater amount of exposed inner surfaces and edges for modification sites. Thus, the observed superior values of turn-on and threshold field, and extraction of high emission current density at lower applied electric field is attributed to the synergic effect of: (a) an optimum length and density combination to overcome screening effect, (b) sharp closed tips and (c) open edges on the outer surface of CNTs which enhance the local field²⁶⁻²⁸. These open edges also act as additional emission sites²⁹. Moreover, other favorable conditions for enhanced emission of such periodic structured conical CNTs could be: (a) hydrogen saturation of open edges on the surface which also decrease the effective work function, (b) nano-sized radius of curvature and (c) highly ordered distribution of the emitters over the whole area of specimen. The cup morphology increases the specific surface area of the sample which reduces the effective density and hence an extremely reduced electric field screening.^{30,31} Furthermore, the formation of sharp bends at the bottom caps where carbon atoms show sp³ like atomic bonds instead of sp² configuration³². This change in coordination would decrease the height of potential barrier and hence could explain the very low work function as can be estimated from the Fowler-Nordheim plots. As predicted, the H- or O- terminated edges greatly effects the net work function. Simulation studies predict the work function of 6.3 eV for a clean edge graphene as compared to the work functions of 3.31 and 7.29 eV respectively for H- and O-terminated edge.³³ Thus, the observed superior values of turn-on and threshold field, and extraction of high emission current density at lower applied electric field is attributed synergic effect of low aspect ratio, sharp diameter of the cups, uniform distribution of the emitters over the whole area of specimen and lower screening effect of the CNCs.^{30,31} However, the performance of CNCs is lower as compared to other carbon based materials, because CNCs nanostructure associated with large number of nano-cup structures in form of array, where each cup have non-uniform dimensions from top to bottom like other carbon materials i.e. CNT. Therefore, the electric field at the base of individual CNCs structures increases the number of emitter points; as a result the overall electric field strength reduces at the base because of enhanced screening effect.^{30,31}

The F-N plot by a plotting the graph of $\ln(J/E^2)$ versus $1/E$ for the CNCs is shown in Figure 4b with a calculated field enhancement factor of ~ 1645 from slope of the linear region of F-N plot. The F-N plot for the CNCs field emitter is nearly linear and shows a tendency for saturation at high electric fields. The field enhancement factor can give idea of the enhancement of the electric field at the emitter sites due to sharp edges with their huge nanometric protrusions. In the present case, the field enhancement factor is calculated from the slope of the F-N plot and is found to be ~ 1645 by assuming work function (ϕ) of the emitter ~ 5 eV for CNCs. Figure 4c shows the typical long-term current stability (I-t) from a CNCs field emitter recorded at a base pressure of $\sim 1 \times 10^{-8}$ mbar. To increased performance of CNCs in

device applications point of view, cathode requires nearly constant emission current stability, so it is a decisive and important parameter in the fabrication of field emission based nanoelectronic devices. Fig. 4c show the field emission current stability traces for CNCs at $\sim 8 \mu\text{A}$ preset value of current for a sampling interval of 10 seconds recorded over a period of 8 hours. The average emission current is seen to be stable over the duration of the measurement characterized by fluctuations in the form of “spikes”. The appearance of the “spikes” in the emission current is attributed to the field induced adsorption, desorption, and migration of the residual gas molecules on the emitter surface. The striking feature of the field emission behaviour of the CNCs emitter is that the average emission current remains constant over the entire duration and shows no signs of the detrimental effects, signalling its mechanical robustness against ion bombardment and field-induced stress. Figure 4d shows the typical field emission micrograph of the CNCs field emitter recorded at a current density of $\sim 500 \mu\text{A}/\text{cm}^2$ consists of a large number of tiny bright spots indeed emission is from most of the protruding CNCs field emitter. The emission picture of CNC was taken from certain height from top window FED instrument. Therefore, exact distribution of emission intensity cannot be visible as uniform as it is. Thus, this new architecture of CNC encourages for further research to be done establishing CNC as a promising next-generation efficient material for FED devices.

4. Conclusions

In summary, the three-dimensional (3D) porous architectures of CNC array have synthesized using combining anodization and CVD techniques for field emission application. The low turn-on field required to draw a current density of $1 \mu\text{A}/\text{cm}^2$ is found to be $2.30 \text{ V}/\mu\text{m}$ for CNCs. The field emission behavior is observed due to a high field enhancement factor associated with surface protrusions. Owing to the low turn on field and cup-like structure morphology, the CNCs emitter can be utilized for new generation vacuum microelectronics/nanoelectronics and flat panel display applications.

Notes and references

- ^aCSIR - National Physical Laboratory, Dr K S Krishnan Road, New Delhi, 110012, India,
^bDepartment of Physics, Kalindi College, University of Delhi, New Delhi, 110008, India,
^cAcademy of Scientific and Innovative Research (AcSIR), CSIR – National Physical Laboratory campus, New Delhi – 110012,
^dCentre for Advanced Studies in Materials Science and Condensed Matter Physics, Department of Physics, University of Pune, Pune 411007, India, ^eDepartment of Advanced functional thin films, surface technology division, Korea institute of material science (KIMS), 797 Changwondaero, Sungsan-GU, Changwon, Gyeongnam, 642-831, Republic of Korea,
^fDepartment of Chemistry, Pittsburg State University, Pittsburg, KS, 66762, USA, ^gPhysical & Materials Chemistry Division, CSIR-National Chemical Laboratory, Pashan Road, Pune 411008, India.
- ^{*} Corresponding author. Tel.: +91-11-45609385, Fx: +91-11-45609310

E-mail address: bipinbhu@yahoo.com (B.K.G.), dj.late@ncl.res.in (D. J. L.), mghahm@kims.re.kr (M.G.H.)

† Electronic Supplementary Information (ESI) available: [details of any supplementary information available should be included here]. See DOI: 10.1039/b000000x/

‡ Footnotes should appear here. These might include comments relevant to but not central to the matter under discussion, limited experimental and spectral data, and crystallographic data.

10

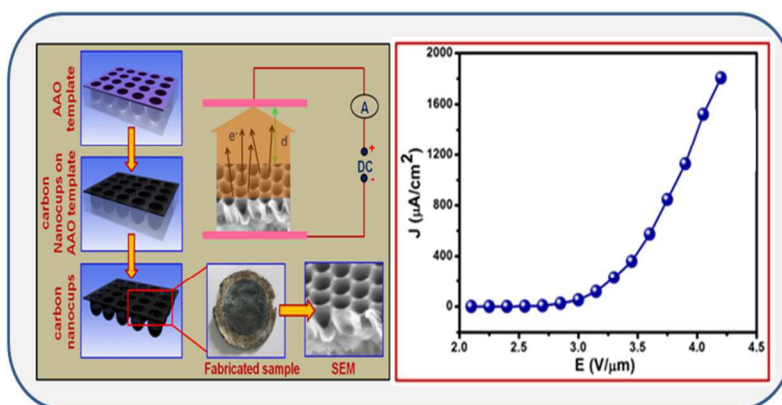
Acknowledgments

The authors wish to thank Director, N.P.L., New Delhi for his keen interest in the work. The authors are thankful to Prof. C. N. R. Rao (JNCASR & ICMS Bangalore) and Prof. O. N. Srivastava (Banaras Hindu University, Varanasi) for encouragement. The authors gratefully acknowledged University Grant Commission (UGC) and Council of Scientific and Industrial Research (CSIR), Govt. of India for financial assistance to carry out this work. This study was supported by the Fundamental Research Program (PNK4060) of the Korean Institute of Materials Science (KIMS). M. G. H. is grateful for the support from the Basic Science Research Program of the National Research Foundation of Korea (NRF) funded by the Ministry of Science, ICT & Future Planning (NRF-2014R1A1A1006214).

References

- R. H. Fowler and L. Nordheim, *Procee. of the Royal Society of London. Series A*, 1928, **119**, 173.
- R. G. Forbes, *Nanotech.*, 2012, **23**, 095706.
- Y. Agrawal, G. Kedawat, P. Kumar, J. Dwivedi, V. N. Singh, R. K. Gupta and B. K. Gupta, *Sci. rep.* 2015, **5**, 11612.
- R. C. Smith, W. M. Tsang, and D. C. Cox and S. R. P. Silva, *App. Phys. Letters*, 2005, **87**, 103112.
- J. S. Suh, K. S. Jeong, J. S. Lee and I. Han. *App. Phys. Letters*, 2002 **80**, 2392.
- H. Chun, M. G. Hahm, Y. Homma, R. Meritz, K. Kuramochi, L. Menon, L. Ci, P.M. Ajayan and Y. J. Jung. *ACS Nano*, 2009, **3**, 1274–1278.
- Q. Liu, W. Ren, Z. G. Chen, L. Yin, and F. Li, H. Cong and H.-M. Cheng. *Carbon*, 2009, **47**, 731-736.
- W. Wang, X. Qin, N. Xu, and Z. Li, *J. App. Phys.*, 2011, **109**, 044304.
- W. Lei, C. Li, M. T. Cole, K. Qu, and S. Ding, *Carbon*, 2013, **56**, 255-263.
- M. Endo, Y. A.Kim, T. Hayashi, Y. Fukai, and K. Oshida, M. Terrones, T.Yanagisawa, S. Higaki and M. S. Dresselhaus. *Appl. Phys. Lett.*, 2002, **80**, 1267-1269.
- Y. A.Kim, T. Hayashi, Y. Fukai, M. Endo, T. Yanagisawa, and M. S. Dresselhaus. *Chem. Phys. Lett*, 2002, **355**, 279–284.
- W. Wang, B. zeng, J. Yang, B. Poudel, J. Huang, M. J. Naughton, and Z Ren, *Adv. Mater.* 2006, **18**, 3275-3278.
- Y. Liu, Y. Xie, J. Chen, J. Liu, C. Gao, *J. Am. Ceram. Soc.*, 2011, **94**, 4387-4390.
- C. L. Liu, H. Gao, L. Li, X. Liu, Q. Gao, H. X. Cuo, T. T. Chen and G. Q. Miao, *RSC Advances*, 2013, **3**, 26149-26152.
- K. Saito, M. Ohtani, S. and Fukuzumi, *J. Am. Chem. Soc.*, 2000, **128**, 14216–14217.
- M. S. Dresselhaus, and P. C. *Adv. Phys*, 2000, **49**, 705-814.
- M. Endo, Y. A. Kim, M. Ezaka, K. Osada, T. Yanagisawa, Takuya Hayashi, Marucio Terrones, and Mildred S. Dresselhaus. *Nano lett*, 2003, **3**, 723–726.
- A. P. Singh, M. Mishra, D. P. Hashim, T. N. Narayanan, M. G. Hahm, P. Kumar, J. Dwivedi, G. Kedawat, A. Gupta, B.P. Singh, A. Chandra, R. Vajtai, S.K. Dhawan, P.M. Ajayan and B.K. Gupta. *Carbon*, 2015, **85**, 79-88.
- K. N. Kudin, B. Ozbas, H. C. Schniepp, R. K. Prud'homme, I. A. Aksay and R. Car. *Nano Lett.*, 2008, **8**, 36-41.
- M. G. Hahm, A. Leela Mohana Reddy, D. P. Cole, M. Rivera, J. A. Vento, J. Nam, H. Y. Jung, Y. L. Kim, T.N. Narayanan, D. P. Hashim, C. Galande, Y. J. Jung, M. Bundy, S. Karna, P. M. Ajayan and R. Vajtai. *Nano Lett.*, 2012, **12**, 5616-5621.
- A. Yadav, G. Kedawat, P. Kumar, A. Anshul, A. D. Deshmukh, O.P. Singh, R.K. Gupta, S. S. Amritphale, G. Gupta, V. N. Singh and B. K. Gupta. *Nanoscale*, 2015, **7**, 12498-12509.
- A. K.Samantara, D. K. Mishra, S. R. Suryawanshi, M. A. More, R. Thapa, D. J. Late, B.K. Jena and C. S. Rout. *RSC Adv*, 2015, **5**, 41887-41893.
- S. R., Suryawanshi, A. K. Singh, M. Deo, D. J. Late, S. Sinha and M. A. More. *Cryst. Eng. Comm*, 2015, **17**, 3936-3944.
- S. R. Suryawanshi, S. S. Warule, S. S. Patil, K. R. Patil, and M. A. More, *ACS App. Mater. Interfaces*, 2014, **6**, 2018-2025.
- C. S. Rout, P. D. Joshi, R. V. Kashid, D. S. Joag, M. A. More, A. J. Simbeck, M. Washington, S. K. Nayak and D. J. Late. *Sci. Rep.*, 2013, **3**, 1-4.
- Y. Saito, and S. Uemura, *Carbon*, 2000, **38**, 169-182.
- J. M. Bonard, J. P. Salvetat, T. Stockli, W. A. D. Heer, L. Forro and A. Châtelain. *Appl. Phys. Lett.*, 1998, **73**, 918.
- S. K. Srivastava, V. D. Vankar, and V. Kumar, *Nanoscale Res. Lett.*, 2008, **3**, 25–30.
- R. Sen, B. C. Satishkumar, A. Govindaraj, K. R. Harikumar and G. Raina, J.-P. Zhang, A.K. Cheetham and C.N.R. Rao. *Chem. Phys. Lett.*, 1998, **287**, 671-676.
- S. Chatterjee, M. Kumar, A. Pal, I. Thakur and T. Som, *J. Mater. Chem. C*, 2015, **3**, 6389-6394.
- I. Chakraborty and P. Ayyub, *Nanotechnology*, 2012, **23**, 015704(7pp).
- J. M. Bonard, H. Kind, T. Stockli, and L. O. Nilsson, *Solid State Elec.*, 2001, **45**, 893-914.
- R. Ramprasad, P. von Allmen and L. R. C. *Phys. Rev. B*, 1998, **6**, 6023-6027.

Graphical Table of Contents (TOC)



A novel strategy for the synthesis of highly ordered low-aspect ratio carbon nanocup arrays and its field emission properties.